

Enhanced coherent control of carrier and spin density in a zinc-blende semiconductor by cascaded second-harmonic generation

Martin J. Stevens

Laboratory for Photonics and Quantum Electronics, 138 IATL, University of Iowa, Iowa City, Iowa 52242

R. D. R. Bhat

Department of Physics, University of Toronto, 60 Saint George Street, Toronto, Ontario M5S 1A7, Canada

X. Y. Pan

Laboratory for Photonics and Quantum Electronics, 138 IATL, University of Iowa, Iowa City, Iowa 52242

H. M. van Driel and J. E. Sipe

Department of Physics, University of Toronto, 60 Saint George Street, Toronto, Ontario M5S 1A7, Canada

Arthur L. Smirl^{a)}

Laboratory for Photonics and Quantum Electronics, 138 IATL, University of Iowa, Iowa City, Iowa 52242

(Received 20 December 2004; accepted 31 January 2005; published online 20 April 2005)

Phase- and polarization-dependent optical processes involving pulses with frequencies ω and 2ω can be used to independently control electron and spin density in zinc-blende semiconductors such as GaAs. One such process is quantum interference control (QUIC) where interference between transition amplitudes associated with one- and two-photon absorption alters the carrier/spin generation rate. A second process, which has been acknowledged but not utilized, is cascaded second-harmonic (CASH) generation in which phase-dependent upconversion/downconversion between the two pulses modulates the 2ω pulse intensity and/or polarization and hence modulates the carrier or spin generation rate by single-photon absorption at 2ω . Here we report the use of (110)-oriented GaAs/AlGaAs quantum wells with a 500-nm AlGaAs buffer layer to enhance CASH and to allow independent control of spin and carrier densities. Experiments conducted with 100-fs pulses at 775 and 1550 nm or at 715 and 1430 nm, with different polarization states and with different sample orientations, show how QUIC and CASH processes vary with excitation frequency and demonstrate the dominant role played by CASH. We point the way to achieving nearly 100% control through CASH. © 2005 American Institute of Physics. [DOI: 10.1063/1.1879079]

I. INTRODUCTION

Over the last decade coherent optical control of electron or exciton density has been demonstrated in bulk, quantum well, and quantum dot semiconductors.^{1–6} In addition, because circularly polarized light can be used to inject spin-polarized carriers,⁷ coherence control of electron spin has also been observed⁶ and may play a key role in the field of semiconductor spintronics.^{8,9} For example, with the appropriate choice of beam polarizations two-color coherent control techniques have been used to *independently* control carrier and spin densities in (111)-oriented bulk GaAs.^{4–6} In these reports,^{4–6} control was attributed to quantum interference control (QUIC) arising from interference between the quantum mechanical transition amplitudes for the two-photon absorption of a fundamental (ω) pulse and the one-photon absorption of a second-harmonic (2ω) pulse.^{4–6,10}

In this paper, by contrast, we report two-color control that is dominated by a cascaded second-harmonic (CASH) process, and we show how CASH can be used to enhance coherent control of carrier and spin densities. Specifically, we demonstrate independent coherent control of carrier density and spin in a (110)-oriented GaAs/AlGaAs multi-

quantum-well (MQW) sample, and we illustrate how the relative amplitudes of CASH and QUIC processes are dependent on optical frequency, beam polarization, and sample orientation. The symmetries of carrier density control and spin control are quite different than for the (111) GaAs used in previous studies,^{4–6} and here we investigate these symmetries in more detail. Owing in part to the long spin lifetimes that have been observed, (110)-GaAs/AlGaAs quantum wells also have shown promise for use in spintronic applications.¹¹ CASH was discussed previously in the context of carrier density control, but was deemed to make a small contribution for the sample used.⁴ For the experimental conditions used here—which are significantly different from those in Ref. 4—we will show that CASH dominates control of both carrier density and spin.

We begin by briefly outlining the basic theoretical concepts behind QUIC and CASH. This is followed by a discussion of the experimental techniques used to observe QUIC–CASH in the (110) MQW sample using femtosecond pulse excitations for different polarizations and at different pairs of frequencies. The data are compared with the theoretical predictions for polarization- and sample-orientation-dependent control. The last section of the paper summarizes results which provide additional evidence that CASH processes dominate both spin and density control in the sample used

^{a)}Electronic mail: art-smirl@uiowa.edu

here, with a control which is larger than that previously observed and, which, with an appropriate sample design, might allow for optical phase-dependent control approaching 100%.

II. THEORETICAL CONSIDERATIONS

A. QUIC

Following earlier works^{4,5} we consider a two-color field, $E(t) = |E_\omega| e^{i\phi_\omega} e^{-i\omega t} \hat{e}_\omega + |E_{2\omega}| e^{i\phi_{2\omega}} e^{-i2\omega t} \hat{e}_{2\omega} + \text{c.c.}$, consisting of a fundamental beam at frequency ω and polarization \hat{e}_ω and a copropagating second-harmonic beam with frequency 2ω and polarization $\hat{e}_{2\omega}$. This beam is incident on a semiconductor with band-gap energy E_g with the frequencies chosen to satisfy $\hbar\omega < E_g < \hbar 2\omega$. The local carrier density injection rate can then be written as⁴⁻⁶

$$\dot{n} = \dot{n}_{2\omega} + \dot{n}_\omega + \dot{n}_I. \quad (1)$$

The first two terms on the right-hand side refer, respectively, to the single- and two-photon generation rates when acting independently. The single-photon absorption rate is $\dot{n}_{2\omega} = 2\varepsilon_0 \hbar^{-1} \text{Im} \chi_1^{ij} |E_{2\omega}^i|^2$, where χ_1 is the linear susceptibility at 2ω ; a related expression exists for the two-photon absorption rate involving χ_3 , the third-order nonlinear susceptibility tensor. The term \dot{n}_I arises from the interference between the quantum mechanical transition amplitudes for one- and two-photon absorption and represents a carrier density control that can enhance or suppress the generation rates associated with single- or two-photon absorption. The interference term can be expressed as

$$\dot{n}_I = \xi_I^{ijk} E_\omega^{i*} E_\omega^j E_{2\omega}^k + \text{c.c.}, \quad (2)$$

where the indices i, j , and k represent Cartesian components of the fields with repeated indices summed over. The \dot{n}_I depends on the polarizations of the ω and 2ω beams and on the phase difference $\Delta\phi \equiv 2\phi_\omega - \phi_{2\omega}$. The density control tensor ξ_I is related to the imaginary part of a second-order susceptibility:^{4,12} $\xi_I^{ijk} = 2\varepsilon_0 \hbar^{-1} \text{Im} \chi_2^{kij}(-2\omega; \omega, \omega)$.

We can similarly write an expression for the local generation rate for spin density polarized along the i direction as

$$\dot{S}^i = \dot{S}_{2\omega}^i + \dot{S}_\omega^i + \dot{S}_I^i. \quad (3)$$

The first term represents generation associated with single-photon absorption and can be written as $\dot{S}_{2\omega}^i = \zeta_1^{ijk} E_{2\omega}^{j*} E_{2\omega}^k$; a related expression involving a fifth-rank tensor exists for spin generation via two-photon absorption. Like the $\text{Im} \chi_1$ tensor, for materials with cubic symmetry, ζ_1 has one independent component. The properties of ζ_1 follow from the usual optical selection rules, which dictate that circularly polarized light injects spin-polarized carriers.^{6,7} The third term in Eq. (3) is related to the quantum interference between the single- and two-photon processes with

$$\dot{S}_I^i = \zeta_I^{ijkl} E_\omega^{j*} E_\omega^k E_{2\omega}^l + \text{c.c.} \quad (4)$$

The tensors ξ_I , and ζ_I reflect properties of the crystal including its symmetry. In GaAs, because of differences in the ξ_I and ζ_I tensors, carrier and spin density can be independently controlled. For crystals with T_d symmetry (e.g.,

GaAs) ξ_I has only one independent component, ξ_I^{abc} , where a, b , and c indicate the directions [100], [010], and [001], or their permutations.⁴ For materials with T_d symmetry, the spin control pseudotensor ζ_I has two independent components,⁶ $\zeta_{IA} \equiv \text{Im} \zeta_I^{abba}$ and $\zeta_{IB} \equiv \text{Im} \zeta_I^{abab}$. In a sense, ζ_I can be thought of as the difference between the “spin-up” and “spin-down” pieces of $\text{Im} \chi_2$.

B. CASH

In contrast to QUIC, CASH is a nonlocal process that causes an enhancement or suppression of the carrier and spin density as the result of a phase-dependent indirect energy transfer from the optical beams to the semiconductor via a cascaded process associated with the real or imaginary part of the second-order susceptibility χ_2 .

If the cascade is associated with the $\text{Re} \chi_2$, the first step in this cascade is the direct transfer of energy between the 2ω and ω beams as a result of frequency up- or down-conversion in the sample. This conversion process does not involve direct energy exchange with the crystal, but because of its $\Delta\phi$ dependence, it leads to a phase-dependent modulation of the 2ω field. In turn, this modulation of the 2ω field can produce a phase modulation of the one-photon injection of carrier density, $\dot{n}_{2\omega}$, which depends on the 2ω intensity, and the carrier spin density generation rate, $\dot{S}_{2\omega}$, which depends on the 2ω polarization state. (In principle, of course, this frequency conversion process also modulates the ω beam; however, under our experimental conditions where the amplitude of the ω beam is much larger than that of the 2ω beam, the cascade process induces very small fractional changes in the ω beam, and thus, for simplicity, this discussion ignores the resulting modulations of \dot{n}_ω and \dot{S}_ω .) Thus, if the 2ω intensity is modified by second-harmonic generation (SHG) the carrier density will be modulated. If its polarization state is modified, the carrier spin density will be modulated. This process is a cascade in the sense that a frequency conversion process is followed by a direct absorption process (i.e., $\text{Re} \chi_2$ followed by $\text{Im} \chi_1$). It is interesting to note that the second step in this cascade requires $E_g < 2\omega$, but the first step does not. Consequently, the two steps in this cascade process can be completely separated and can occur in different materials within the same sample, or the frequency conversion can take place external to the sample in a separate crystal.

Similarly, there is also a cascaded process associated with the $\text{Im} \chi_2$. The first step in this cascade is the QUIC process described in Sec. II A. QUIC produces a phase-dependent enhancement or suppression of the 2ω and the ω energy directly deposited in the sample, which in turn produces a modulation of the 2ω intensity or polarization, which will result in a modulation of the carrier density through one-photon absorption of 2ω or a modulation of the spin density through one-photon spin injection by 2ω . Thus, the cascade associated with the $\text{Im} \chi_2$ is a QUIC process followed by a direct absorption process (i.e., $\text{Im} \chi_2$ followed by $\text{Im} \chi_1$). In contrast to the cascade associated with the $\text{Re} \chi_2$, both steps in this cascade require $E_g > 2\omega$, and cannot be fully separated.

TABLE I. Calculated QUIC contributions to carrier density control and spin control. CASH predictions can be found by changing the ξ and ζ constants, setting $r=0$, and modifying $\Delta\phi$.

Polarizations		Carrier density control	Spin control
ω	2ω	$\dot{n}_l = 2\xi_I^{abc} E_{2\omega} E_\omega ^2 \times$	$\dot{S}_l^z = (\zeta_{IA} + 2\zeta_{IB}) E_{2\omega} E_\omega ^2 \times$
\hat{x}	\hat{x}	$-3 \sin^2 \alpha \cos \alpha \cos \Delta\phi$	$\sin \alpha (3 \cos^2 \alpha - 1) \sin \Delta\phi$
\hat{x}	\hat{y}	$\sin \alpha (3 \cos^2 \alpha - 1) \cos \Delta\phi$	$(r + 3 \sin^2 \alpha) \cos \alpha \sin \Delta\phi$
$\hat{\sigma}^-$	$\hat{\sigma}^+$	$(3/2\sqrt{2}) \cos \Delta\phi$	$(3/2\sqrt{2}) \cos \Delta\phi$
$\hat{\sigma}^-$	$\hat{\sigma}^-$	$-(1/2\sqrt{2}) \cos \Delta\phi$	$(1/2\sqrt{2})(1 + 2r) \cos \Delta\phi$

Because the cascaded SHG process is spatially distributed and does not necessarily occur where the one-photon absorption processes do, an analysis of CASH must account for propagation effects. Nevertheless, we can understand the symmetry properties of these processes by writing tensor expressions for the CASH contributions to carrier and spin density control. If the ω field is not depleted, these expressions are very similar to Eqs. (2) and (4):

$$\Delta \dot{n}_{2\omega} = \xi_C^{ijk} E_\omega^{i*} E_\omega^{j*} E_{2\omega}^k + \text{c.c.}, \quad (5)$$

$$\Delta S_{2\omega}^i = \zeta_C^{ijkl} E_\omega^{j*} E_\omega^{k*} E_{2\omega}^l + \text{c.c.}, \quad (6)$$

where the electric-field amplitudes are those incident on the sample. The effective cascaded tensors can be written as $\xi_C^{ijk} \propto (\text{Im} \chi_1^{km}) \chi_2^{mij}$ and $\zeta_C^{ijkl} \propto \zeta_1^{iml} \chi_2^{mjk}$ and can incorporate propagation effects. Since χ_1 is effectively a scalar in a material with T_d symmetry, ξ_C has the same symmetry as ξ_I , and the QUIC and CASH contributions to *density* control cannot be distinguished by symmetry considerations alone. For spin control, since ζ_I has only one independent component for a material with T_d symmetry, the cascaded tensor has one independent complex component, ζ_C^{abab} ; it has the same symmetry properties as ζ_I only if $\zeta_{IA} = 0$. In general ζ_{IA} depends on ω . Therefore, QUIC and CASH contributions to spin control can have the same or *different* dependences on polarizations and sample orientation, depending on the value of ζ_{IA} .

C. QUIC and CASH in [110] GaAs

We have used Eqs. (2) and (4)–(6) to calculate carrier and spin density control for ω and 2ω pulses propagating along the [110] axis in bulk GaAs. For α defined as the angle between the laboratory x axis and the [001] crystallographic axis, Table I shows the expected values for QUIC as a function of α and $\Delta\phi$ for four different polarization configurations. To simplify the expressions, we define $r \equiv -2\zeta_{IA}/(\zeta_{IA} + 2\zeta_{IB})$.

The CASH predictions for carrier density control ($\Delta \dot{n}_{2\omega}$) can be found from Table I by changing ξ_I^{abc} to ξ_C^{abc} and changing $\Delta\phi$ to $\Delta\phi + \delta_p$, where δ_p is a phase that incorporates propagation effects. To find the CASH predictions for spin control ($\Delta \dot{S}_{2\omega}^z$) from Table I, we can substitute $|\zeta_C^{abab}|$ for ζ_{IB} , set $\zeta_{IA} = 0$ (hence $r = 0$), and change $\Delta\phi$ to $\Delta\phi + \delta_s$, where δ_s is a phase related to propagation effects. Since propagation effects are included, the parameters ξ_C^{abc} , $|\zeta_C^{abab}|$, δ_p , and δ_s all depend on sample structure and excitation conditions.

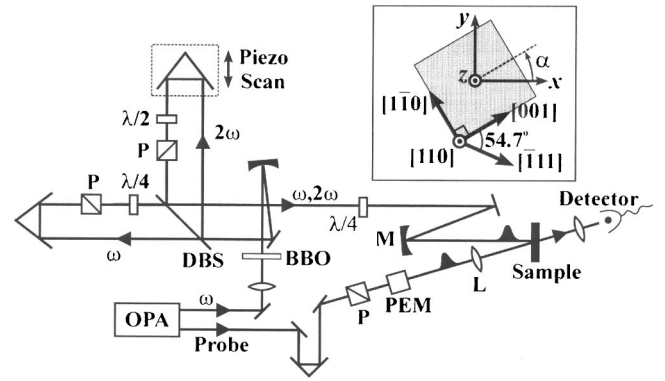


FIG. 1. Experimental geometry: BBO generates 2ω ; DBS is a dichroic beam splitter; P, $\lambda/2$, and $\lambda/4$ are a polarizer, half-wave plate, and quarter-wave plate; PEM is a photoelastic modulator; L and M are a lens and a curved mirror. Inset: schematic of sample showing crystallographic directions and laboratory coordinate system. The angle between x and [001] is α .

Note that for density control, QUIC and CASH have equivalent α dependence, but for spin control, QUIC has a different α dependence than CASH for $r \neq 0$.

III. EXPERIMENTAL TECHNIQUES

For the experiments we use the setup illustrated in Fig. 1. The ~ 100 -fs fundamental (ω) pulse, with wavelength centered at 1.55 or 1.43 μm , is generated in an optical parametric amplifier (OPA) that is pumped by a Ti:Sapphire laser-seeded regenerative amplifier operating at 250 kHz. SHG in beta barium borate (BBO) produces 2ω pulses at 0.775 or 0.715 μm . A scanning dichroic Michelson interferometer controls the phase difference $\Delta\phi$, and the polarization of each pulse is independently controlled with wave plates and polarizers. The two pump pulses are recombined collinearly, are temporally overlapped, and are focused at normal incidence onto the semiconductor sample.

The probe pulse, with a wavelength of 0.81 μm , is derived from the output of the regenerative amplifier after it has been used to pump the OPA, and it monitors the density and spin of pump-injected carriers. The probe is spatially centered on the pump spots and arrives ~ 3 ps after the pumps, after the carriers thermalize but before the spins of the electrons relax.

The sample¹³ is a MQW structure consisting of 20 periods of 8-nm-wide GaAs wells ($E_g \approx 1.45$ eV) alternating with 8-nm-thick $\text{Al}_{0.3}\text{Ga}_{0.7}\text{As}$ barriers ($E_g \approx 1.80$ eV), originally grown on a (110)-oriented GaAs substrate with an $\text{Al}_{0.3}\text{Ga}_{0.7}\text{As}$ etch stop layer grown between the MQW and the substrate. The MQW is glued to a glass window, and the GaAs substrate has been removed with a selective etch, leaving an ~ 500 -nm-thick $\text{Al}_{0.3}\text{Ga}_{0.7}\text{As}$ etch stop layer on top of the MQW. This sample is held at room temperature, and can be rotated about the [110] axis, as the Fig. 1 inset shows. The 2ω and ω irradiances are typically and ~ 190 MW/cm^2 and ~ 14 GW/cm^2 , respectively. The carrier density resulting from the one-photon absorption of 2ω is $n_{2\omega} \approx 7 \times 10^{17} \text{ cm}^{-3}$, and the density from the two-photon absorption of ω is $n_\omega \approx (7-10) \times 10^{17} \text{ cm}^{-3}$, where the latter depends on ω polarization and angle α .¹⁴

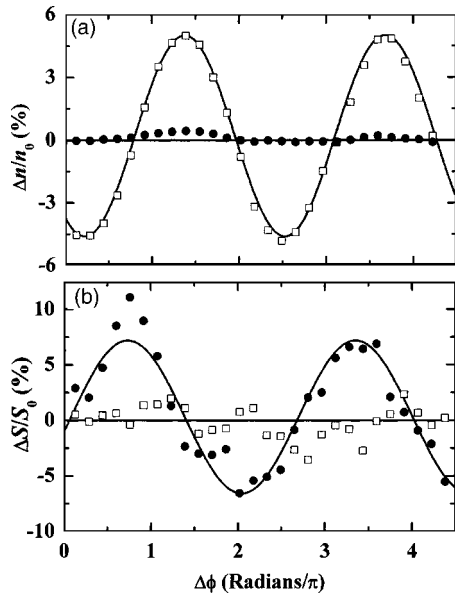


FIG. 2. Measured fractional change in (a) carrier density and (b) spin density for orthogonal linear excitation with 1.55 and 0.775- μm pump-beams for $\alpha=55^\circ$ (\bullet) and 95° (\square). The solid curves are sinusoidal fits to the data.

To monitor the $\Delta\phi$ -dependent change in carrier density Δn , we measure the phase-dependent differential probe transmission, $\Delta T(\Delta\phi)$, using a linearly polarized probe pulse, which is equally sensitive to carriers with spins along $+z$ and $-z$. This signal is normalized¹⁵ by the differential transmission induced by the average background carrier density, $n_0 = \langle n_{2\omega} \rangle + \langle n_\omega \rangle$, where $\langle \rangle$ denotes an average over $\Delta\phi$.

To monitor the $\Delta\phi$ -dependent change in net spin along the z axis, ΔS , we use circular probe polarizations, since a left-circularly ($\hat{\sigma}^-$) or right-circularly ($\hat{\sigma}^+$) polarized probe pulse is most sensitive to saturation of carriers with spins along $+z$ or $-z$, respectively.^{7,16} To find ΔS , we measure $\Delta T(\Delta\phi)$ as the probe polarization is modulated between $\hat{\sigma}^-$ and $\hat{\sigma}^+$ with a photoelastic modulator. This quantity is normalized by the measured average total spin injected when both 2ω and ω pulses are $\hat{\sigma}^-$ polarized, $S_0 = \langle S_{2\omega(\hat{\sigma}^-)}^z \rangle + \langle S_{\omega(\hat{\sigma}^-)}^z \rangle$.

IV. POLARIZATION- AND SAMPLE-ORIENTATION-DEPENDENT CONTROL

In the first set of experiments with 1.55–0.775- μm pump beams ($\Delta E = \hbar 2\omega - E_g = 150$ meV for GaAs) entering the MQW after passing through the AlGaAs layer, we measured the change in carrier density Δn and spin ΔS as a function of the phase $\Delta\phi$ while systematically rotating the sample. Four pump polarization combinations were used: orthogonal linear, parallel linear, same circular, and opposite circular.

Figure 2 illustrates typical measurements of $\Delta n/n_0$ and $\Delta S/S_0$ as a function of the $\Delta\phi$ phase¹⁷—in this case for orthogonal linear polarizations (with \hat{e}_ω polarized along x and $\hat{e}_{2\omega}$ along y) and for two sample orientations: $\alpha=95^\circ$ and $\alpha=55^\circ$. At $\alpha=95^\circ$, \hat{e}_ω is nearly polarized along $[\bar{1}10]$; for this orientation, there is a large density control signal but little or no periodic modulation of the spin, at least within the noise level of the data. By contrast, at $\alpha=55^\circ$, for which \hat{e}_ω is approximately parallel to $[\bar{1}11]$, the phase $\Delta\phi$ controls the spin, but density control is nearly zero. The amplitudes of the sinusoidal fits to the phase-dependent $\Delta n/n_0$ and $\Delta S/S_0$ data were extracted and are plotted in Figs. 3(a) and 3(b), respectively, along with the peak amplitudes extracted in a similar fashion for other sample orientations. These data show dramatic variation as a function of α . Clearly, for fixed orthogonal linear polarizations, we can choose a sample orientation to control the density only ($\alpha \approx 90^\circ, 270^\circ$), the spin only ($55^\circ, 135^\circ$, etc.), both ($30^\circ, 80^\circ, 110^\circ, 150^\circ$, etc.), or neither ($0^\circ, 180^\circ$).

In contrast, for *parallel* linear excitation (both \hat{e}_ω and $\hat{e}_{2\omega}$ along \hat{x}), the α dependences of density control and spin control are reversed, as evidenced by the data in Figs. 3(c) and 3(d). Hence, at a fixed sample orientation such as 55° , we can choose parallel pump polarizations to control density but not spin, or we can choose orthogonal polarizations to control spin but not density. At another fixed orientation such as $\alpha \approx 90^\circ$, this result is reversed, and parallel polarizations control spin, while orthogonal polarizations control density. Finally, the data in Figs. 3(e) and 3(f) show that for either opposite circular (\hat{e}_ω is $\hat{\sigma}^-$, $\hat{e}_{2\omega}$ is $\hat{\sigma}^+$) or same circular (both $\hat{\sigma}^-$) excitation, *both* density and spin can be controlled—

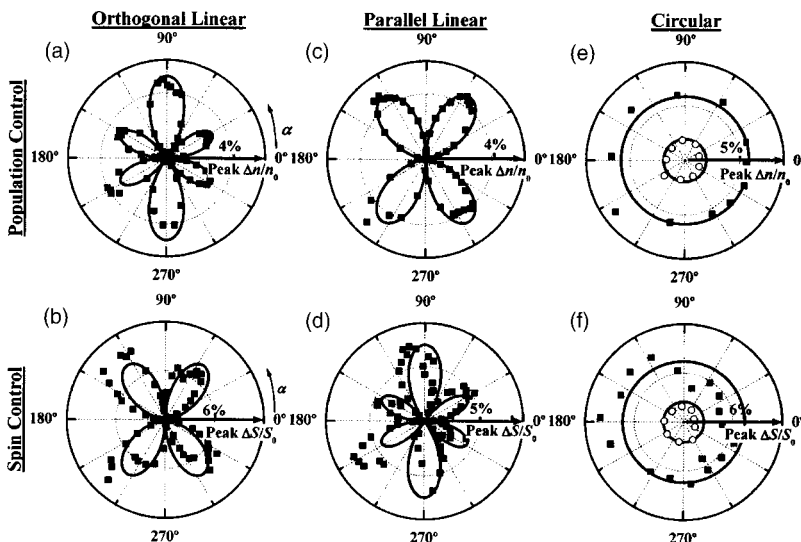


FIG. 3. Top row: measured peak phase-dependent carrier density control. Bottom row: measured peak spin control. The ω and 2ω pulse polarizations are (a) and (b) orthogonal linear, (c) and (d) parallel linear, and (e) and (f) opposite circular (solid squares) and same circular (open circles). All the data are taken with $\Delta E = 150$ meV. The solid curves are simulations of CASH and of QUIC (for $r=0$).

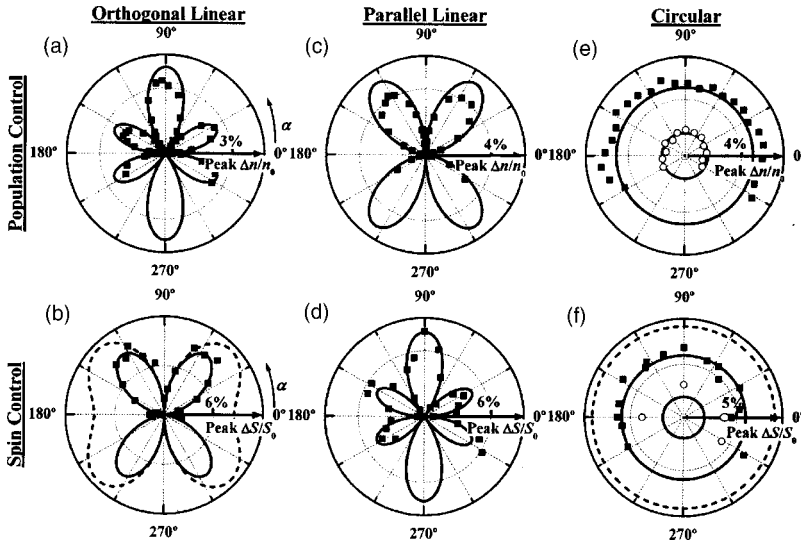


FIG. 4. Same as Fig. 3, except the data are taken with $\Delta E=280$ meV. CASH simulations (solid curves) use a single value of $|\xi_C^{abab}|$ and a single value of ξ_C^{abc} for all polarizations. QUIC simulations (for $r=1.7$) are represented by the dashed curves in (b) and in (f) for the same circular polarizations; otherwise, QUIC simulations are also represented by the solid curves.

independent of sample angle. The data in Figs. 2 and 3 therefore illustrate that several parameters can be used to independently control carrier density and spin, including the phases and polarizations of the excitation fields and the orientation of the semiconductor crystal.

To compare the experimental results to the QUIC and CASH theories, we refer to Table I. Interestingly, the α dependence of the expressions in the first two rows of Table I (for $r=0$)—as well as the data in Figs. 3(a)–3(d)—match those for the parallel and perpendicular components of SHG from (110) GaAs that were first measured more than 40 years ago.¹⁸ This is not surprising since ξ_1 has the symmetry of χ_2 . However, Ducuing and Bloembergen measured only SHG, not the coherent control of carrier density and spin. The component of the second-harmonic beam with the same polarization as the incident 2ω pulse leads to density control, while the component of the second-harmonic beam whose polarization is orthogonal to the incident 2ω pulse leads to spin control.

To compare the Table I expressions with the experimental results, simulations of CASH are plotted in Fig. 3 using a single value of $|\xi_C^{abab}|$ and the best-fit value of ξ_C^{abc} for each data set (although ξ_C^{abc} is varied no more than 20% from its mean value). For all polarization configurations, the CASH theory reproduces all of the essential features of the data without requiring special constraints on any parameter. The QUIC theory, by contrast, agrees with these data only if r is approximately zero. Fourteen-band calculations¹⁹ of the spin control tensor elements predict that, although ξ_{IA} and ξ_{IB} are slowly varying functions of ΔE , they do pass through zero.²⁰ As a result, the magnitude and sign of r should depend strongly on electron kinetic energy. The ΔE used for the measurements shown in Fig. 3 (i.e., $\Delta E=150$ meV) was chosen so that r is small ($r=0.012$). Under these conditions, CASH and QUIC predict the same dependence on sample orientation. Consequently, the data in Fig. 3 provide no information about which process dominates.

V. CASH VERSUS QUIC: FREQUENCY DEPENDENCE

To help determine whether CASH or QUIC is the dominant process for our sample, spin and density control experi-

ments with 0.715- and 1.43- μm pulses ($\Delta E \approx 280$ meV) were undertaken. The results are shown in Fig. 4 as a function of α , albeit over a more limited range: $-30 < \alpha < 210$. The results are very similar to those in Figs. 2 and 3—both qualitatively and quantitatively. The predictions of the CASH theory of coherent control of population and spin acting alone are shown by the solid curves in Fig. 4, and they again provide good agreement with the data.

Expectations for the QUIC theory, as given in Table I, however, are significantly different for $\Delta E \approx 280$ meV, where our 14-band calculations of the spin control tensor predict $r=1.7$. All of the QUIC carrier density control terms and the QUIC spin control terms for parallel linear and for opposite circular polarization are independent of r . Consequently, the solid curves in Figs. 4(a) and 4(c)–4(e) and also represent the QUIC predictions. The QUIC calculations for the spin control for orthogonal linear ($\hat{x}\hat{y}$) and same circular ($\hat{\sigma}^-\hat{\sigma}^-$) polarizations are shown by the dashed lines in Figs. 4(b) and 4(f), and they differ significantly from the CASH predictions. For example, for $\hat{x}\hat{y}$ polarizations, CASH predicts no spin control at 0° and 180° , while QUIC predicts substantial control. Also, at $\Delta E=280$ meV, QUIC predicts that spin control for $\hat{\sigma}^-\hat{\sigma}^-$ should be 1.5 times *larger* than for $\hat{\sigma}^-\hat{\sigma}^+$, while CASH predicts that it should be 3 times *smaller*. In addition, QUIC predicts that spin control for $\hat{\sigma}^-\hat{\sigma}^+$ excitation should be ~ 2.9 times *larger* than for $\hat{\sigma}^-\hat{\sigma}^-$ excitation at $\Delta E=150$ meV, but, by contrast, that it should be 1.5 times *smaller* at $\Delta E=280$ meV. Alternatively, if CASH acts alone, these behaviors should be *independent* of ΔE : spin control for $\hat{\sigma}^-\hat{\sigma}^+$ excitation should be exactly 3 times *larger* than for $\hat{\sigma}^-\hat{\sigma}^-$. All of the tendencies in the data strongly indicate that CASH dominates spin control.

VI. QUIC VERSUS CASH: DEPENDENCE ON PROPAGATION DIRECTION

We can obtain additional evidence for the importance of CASH by investigating the dependence of the carrier and spin density control on propagation direction through the sample. First, with the 1.55- and 0.775- μm pulses with opposite circular polarization entering the sample through the

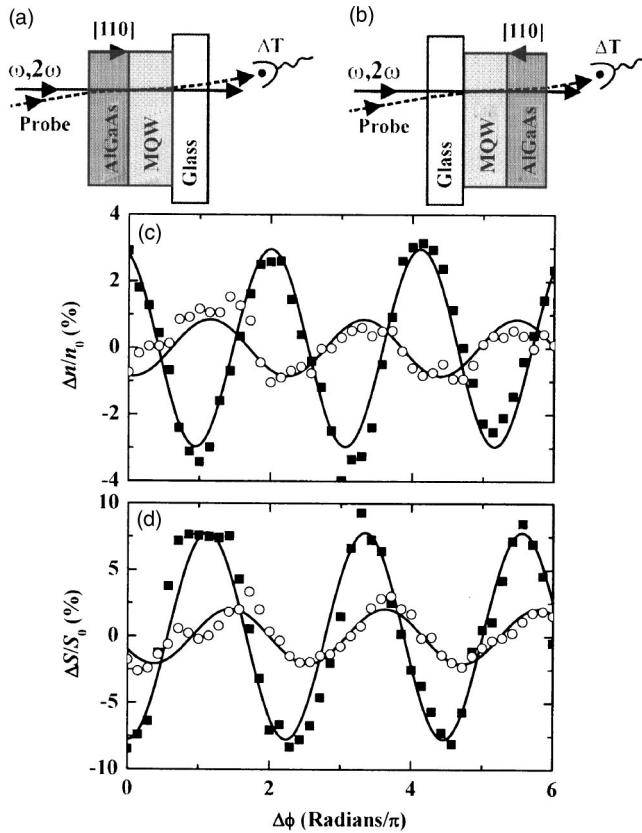


FIG. 5. (a) Excitation geometry used for the data in Figs. 2 and 3: beams enter the sample from the AlGaAs side. (b) Flipped geometry: beams enter from the MQW side. The lower plots show measured (c) density control and (d) spin control for $\hat{\sigma}^- \hat{\sigma}^+$ excitation at $\Delta E \approx 150$ meV. The solid square data are obtained using geometry (a), open circle data using geometry (b).

AlGaAs layer, as illustrated in Fig. 5(a), we measure the fractional changes in charge density, $\Delta n/n_0$, and spin, $\Delta S/S_0$, as a function of phase, $\Delta\phi$; the data are represented by the solid squares in Figs. 5(c) and 5(d). When the beams enter first from the quantum well side, as shown in Fig. 5(b), the carrier density, $\Delta n/n_0$, and spin, $\Delta S/S_0$, measurements are indicated by the open circles in Figs. 5(c) and 5(d).

These results can be understood by recalling that SHG occurs in GaAs and $\text{Al}_{0.3}\text{Ga}_{0.7}\text{As}$, since the real part of χ_2 is nonzero in *both*. By contrast, one-photon absorption of 2ω light and QUIC can occur only if $2\hbar\omega > E_g$, where $\text{Im}\chi_2$ and ζ_I are nonzero. Thus, for a $0.775\text{-}\mu\text{m}$ ($\hbar 2\omega = 1.6$ eV) pump beam, one-photon absorption of 2ω light and QUIC will occur in the GaAs, but not in the $\text{Al}_{0.3}\text{Ga}_{0.7}\text{As}$ barriers or in the etch stop layer. Thus, when the beams first pass through the $\text{Al}_{0.3}\text{Ga}_{0.7}\text{As}$ [Fig. 5(a)], significant phase-dependent cascaded SHG occurs in this layer—before the 2ω pulse encounters the MQW, where QUIC, additional CASH, and one-photon absorption of 2ω light will occur. In contrast, when the beams enter through the MQWs, CASH still occurs in the $\text{Al}_{0.3}\text{Ga}_{0.7}\text{As}$ etch stop layer, but too late to affect QUIC or the one-photon absorption of 2ω in the MQWs. Clearly, we obtain much larger $\Delta\phi$ -dependent control when using the $\text{Al}_{0.3}\text{Ga}_{0.7}\text{As}$ layer as a kind of a “pre-amplifier,” indicating that the cascaded process dominates both population control and spin control in the configuration shown in Fig. 5(a).

VII. DISCUSSION

We have also performed detailed calculations for density control and spin control that include both QUIC and CASH. These calculations incorporate one-dimensional propagation effects, reflections at dielectric interfaces, and pump depletion in a rigorous manner using Maxwell’s equations, following the method of Fraser *et al.*^{4,5} and modified where necessary to include spin control. The GaAs and AlGaAs layers are treated as bulk material, and the linear and nonlinear optical properties used in these calculations either are experimentally measured values taken from the literature^{4,21–23} or are calculated using a 14-band model.²⁰ We use the ratio $\text{Im}\chi_2/\text{Re}\chi_2 = 0.32$, which was experimentally determined by Fraser *et al.* in bulk GaAs.⁴ These calculations agree very well with the α -dependent data in Fig. 3.

Using these values for the optical properties, however, the propagation calculations do not reproduce the large measured decreases in Δn and ΔS that result from flipping the sample as shown in Fig. 5. Nevertheless, we can obtain reasonably good agreement with the data in Fig. 5 by adjusting the values of $\text{Re}\chi_2$, $\text{Im}\chi_2$, and ζ_I . We have varied these over large ranges, and find that CASH is the dominant mechanism in the samples considered here, for both Δn and ΔS for any choice of these parameters that produces even approximate agreement with these data. Adjusting these and other parameters is reasonable in part because the initial values are taken from bulk material, while the experiments are done in quantum wells. Thus the data in Fig. 5 exhibit a clear indication that CASH dominates both density control and spin control.

In addition, we can use these propagation calculations to corroborate the symmetry analysis of CASH introduced in Sec. II. If we remove the effects of QUIC by setting $\text{Im}\chi_2 = \zeta_I = 0$, the predictions of $\Delta n_{2\omega}$ and $\Delta n_{2\omega}^z$, from these propagation calculations exhibit the same α dependences as those in Table I modified for CASH.

Note that the symmetry predictions in Table I are specific to a bulk zinc-blende semiconductor, such as GaAs, which has T_d symmetry, whereas the (110)-oriented quantum wells used in the experiments have C_{2v} symmetry. However, the T_d predictions can be shown to be special cases of the predictions for C_{2v} . As evidenced by the agreement between data and theory in Fig. 3, the more general bulk theory presented in this paper is a good approximation for the quantum well sample studied here. Furthermore, since CASH dominates density control and spin control, and since the AlGaAs etch stop layer has T_d symmetry, it is not surprising that the data exhibit T_d symmetry.

Finally, we also expect to optically inject *currents* in this geometry due to QUIC^{10,13,24–26} and, if the sample is under some strain, due to the photogalvanic effect.^{26,27} However, the fractional change in carrier density and spin resulting from currents is typically quite small^{28,29} ($\sim 0.1\%$). Spatially resolved measurements (not shown) confirm that the much larger modulations observed in Figs. 2–5 are a measure of phase-dependent changes of the *overall* carrier density and spin. In contrast, previous measurements of QUIC currents^{10,13,25,28} were done with ω and 2ω pulses propagat-

ing along the [001] direction, in which case \dot{n}_I , $\Delta\dot{n}_{2\omega}$, \dot{S}_I^z , and $\Delta\dot{S}_{2\omega}^z$ are all zero.²⁵

VIII. SUMMARY

We have demonstrated independent control of carrier and spin density in (110)-oriented GaAs/AlGaAs quantum wells, effectively decoupling the charge and spin degrees of freedom. Control parameters include the polarizations and phases of the excitation fields and the symmetry and orientation of the semiconductor crystal. The orientation-dependent data cannot distinguish the relative roles of QUIC and CASH for 1.55- and 0.775- μm pump beams; however, for 1.43- and 0.715- μm pump beams, it is clear that CASH dominates spin control at least when the beams first pass through the AlGaAs etch stop layer. In addition, in experiments where the propagation direction through the sample is reversed, we have shown that the phase-dependent control is much stronger when the “preamplifying” AlGaAs layer occurs before the quantum wells, indicating the dominant role of CASH over QUIC for both spin and carrier density control.

The comparison of the experimental data with results from a model incorporating detailed propagation effects demonstrates that CASH dominates both carrier density control and spin control for the sample structure and excitation conditions used here, when the beam first enters through the AlGaAs layer. The more pronounced role for CASH for this sample, as opposed to the earlier works^{4–6} for 650-nm-thick (111)-GaAs sample partly reflects the fact that in the MQW sample $\text{Im}\chi_2$ is nonzero in a relatively smaller volume than $\text{Re}\chi_2$. In future studies, the knowledge from these studies could be used to design a sample and choose the appropriate excitation conditions to enhance the role of either QUIC or CASH. For example, given that the coherence length for CASH is approximately⁵ 1 μm , an even thicker AlGaAs layer could be used to enhance CASH. Taken one step further, with an appropriate SHG phase-matched material as the preamplifier, CASH control approaching 100% might be achievable by converting only $\sim 1\%$ of the incident ω beam to 2ω radiation. This should allow another level of sophistication in the phase control of carrier density and spin in semiconductors, and provide a deeper understanding of the underlying physics.

ACKNOWLEDGMENTS

We thank Eric Gansen, Scot Hawkins, Eric Loren, Ali Najmaie, and Hui Zhao for insightful conversations, and we thank Elias Towe for providing the sample. This work was supported in part by the Office of Naval Research, the De-

fense Advanced Research Projects Agency, Photonics Research Ontario, and the Science and Engineering Research Council of Canada.

- ¹A. P. Heberle, J. J. Baumberg, E. Binder, T. Kuhn, K. Köhler, and K. H. Ploog, *IEEE J. Sel. Top. Quantum Electron.* **2**, 769 (1996).
- ²X. Marie, P. Le Jeune, T. Amand, M. Brousseau, J. Barrau, M. Paillard, and R. Planel, *Phys. Rev. Lett.* **79**, 3222 (1997).
- ³N. H. Bonadeo, J. Erland, D. Gammon, D. Park, D. S. Katzer, and D. G. Steel, *Science* **282**, 1473 (1998).
- ⁴J. M. Fraser, A. I. Shkrebtii, J. E. Sipe, and H. M. van Driel, *Phys. Rev. Lett.* **83**, 4192 (1999).
- ⁵J. M. Fraser and H. M. van Driel, *Phys. Rev. B* **68**, 085208 (2003).
- ⁶M. J. Stevens, R. D. R. Bhat, J. E. Sipe, H. M. van Driel, and A. L. Smirl, *Phys. Status Solidi B* **238**, 568 (2003).
- ⁷*Optical Orientation, Modern Problems in Condensed Matter Sciences*, edited by F. Meier and B. P. Zakharchenya (North-Holland, Amsterdam, 1984), Vol. 8.
- ⁸S. A. Wolf, D. D. Awschalom, R. A. Buhrman, J. M. Daughton, S. von Molnán, M. L. Roukes, A. Y. Chtchelkanova, and D. M. Treger, *Science* **294**, 1488 (2001).
- ⁹*Semiconductor Spintronics and Quantum Computation*, edited by D. D. Awschalom, D. Loss, and N. Samarth (Springer, Berlin, 2002).
- ¹⁰H. M. van Driel and J. E. Sipe, in *Ultrafast Phenomena in Semiconductors*, edited by K.-T. Tsen (Springer, New York, 2001), pp. 261–307, and references therein.
- ¹¹Y. Ohno, R. Terauchi, T. Adachi, F. Matsukura, and H. Ohno, *Phys. Rev. Lett.* **83**, 4196 (1999).
- ¹²J. E. Sipe and A. I. Shkrebtii, *Phys. Rev. B* **61**, 5337 (2000).
- ¹³M. J. Stevens, A. L. Smirl, R. D. R. Bhat, J. E. Sipe, and H. M. van Driel, *J. Appl. Phys.* **91**, 4382 (2002).
- ¹⁴M. D. Dvorak, W. A. Schroeder, D. R. Andersen, A. L. Smirl, and B. S. Wherrett, *IEEE J. Quantum Electron.* **30**, 256 (1994).
- ¹⁵Although $\langle n_\omega \rangle$ is a function of α , as discussed in Ref. 14, the normalization factor n_0 (which never deviates more than 10% from its mean value) is calibrated at one α for each polarization configuration for the data in Fig. 3. For the data in Fig. 4, at each α , n_0 is either measured or interpolated from n_0 measured at surrounding α .
- ¹⁶Because the probe pulse propagates at a very small internal angle ($\sim 3^\circ$) with respect to normal incidence, the change in probe transmission is not sensitive to spins oriented in the x - y plane.
- ¹⁷The relative phase of any two experimental curves cannot be deduced from the data in Figs. 2 or 5, since we did not track interferometer drift between measurements.
- ¹⁸J. Ducuing and N. Bloembergen, *Phys. Rev. Lett.* **10**, 474 (1963).
- ¹⁹P. Pfeffer and W. Zawadzki, *Phys. Rev. B* **53**, 12813 (1996).
- ²⁰R. D. R. Bhat and J. E. Sipe (private communication).
- ²¹I. Shoji, T. Kondo, and R. Ito, *Opt. Quantum Electron.* **34**, 797 (2002).
- ²²E. D. Palik, *Handbook of Optical Constants of Solids*, 1st ed (Academic, Orlando, 1985).
- ²³A. N. Pikhtin and A. D. Yas'kov, *Sov. Phys. Semicond.* **14**, 389 (1980).
- ²⁴A. Najmaie, R. D. R. Bhat, and J. E. Sipe, *Phys. Rev. B* **68**, 165348 (2003).
- ²⁵M. J. Stevens, A. Najmaie, R. D. R. Bhat, J. E. Sipe, H. M. van Driel, and A. L. Smirl, *J. Appl. Phys.* **94**, 4999 (2003).
- ²⁶R. D. R. Bhat, F. Nastos, A. Najmaie, and J. E. Sipe, e-print cond-mat/0404066.
- ²⁷S. D. Ganichev W. Prettl, *J. Phys.: Condens. Matter* **15**, R935 (2003).
- ²⁸M. J. Stevens, A. L. Smirl, R. D. R. Bhat, A. Najmaie, J. E. Sipe, and H. M. van Driel, *Phys. Rev. Lett.* **90**, 136603 (2003).
- ²⁹J. Hübner, W. W. Rühle, M. Klude, D. Hommel, R. D. R. Bhat, J. E. Sipe, and H. M. van Driel, *Phys. Rev. Lett.* **90**, 216601 (2003).